Article

Discovery Medicine 2023; 35(177): 539–552
https://doi.org/10.24976/Discov.Med.202335177.55

Exploring Influenza A Virus-Induced Lung Injury and Immune Response Based on Humanized Lung-on-Chip

Shaoyan Gu[1,2,†], Pan Pan[1,2,†], Jiang Wang[1,2], Yinghan Shi[1,2], Feng Shi[3], Yuhan Zhang[4], Wei Guan[1,2], Yan Cao[1], Haimao Qin[5], Qingzhong Wang[6,*], Lixin Xie[1,2,*]

[1]College of Pulmonary & Critical Care Medicine, 8th Medical Center, Chinese PLA General Hospital, 100091 Beijing, China
[2]Department of Critical Care Medicine, Chinese PLA Medical School, 100853 Beijing, China
[3]Department of Critical Care Medicine, Qiqihar First Hospital, 161000 Qiqihaer, Heilongjiang, China
[4]Department of Pulmonary and Critical Care Medicine, Ruijin Hospital, Shanghai Jiao Tong University School of Medicine, 200025 Shanghai, China
[5]Department of Respiratory and Critical Care Medicine, The People's Hospital of China Three Gorges University, 443000 Yichang, Hubei, China
[6]Department of Clinical Microbiology, Shanghai Centre for Clinical Laboratory, 200126 Shanghai, China
*Correspondence: wangqingzhong@sccl.org.cn (Qingzhong Wang); xielx301@126.com (Lixin Xie)
†These authors contributed equally.
Published: 1 August 2023

Background: Influenza is an important respiratory tract pathogen that causes substantial seasonal and pandemic morbidity and mortality. The aim of this study was to systematically analyze the transcriptome characteristics of peripheral blood mononuclear cells (PBMCs) after influenza A virus infection by constructing a human lung microarray model composed of PBMCs to simulate the influenza A virus infection process.

Methods: A human lung microarray model was constructed using alveolar epithelial cells, vascular endothelial cells, alveolar macrophages and PBMCs, for simulation of the process of influenza A virus infection. The transcriptome characteristics of PBMCs after influenza A virus infection were analyzed by a single-cell RNA sequencing system.

Results: The study could realistically mimic the structure and physiological functions of the alveoli *in vitro* using immunofluorescence staining and expression of the specific marker. After the influenza A virus infected the upper lung chip channels, the epithelial cells underwent a high inflammatory response and spread to endothelial cells. Under experimental conditions, the Influenza A virus infection did not compromise the integrity of epithelial cells, but caused damage to endothelial cells and barrier dysfunction. Single-cell RNA sequencing of PBMCs showed that B and cluster of differentiation 4 (CD4) T cells played important immunomodulatory roles in response to influenza A virus infection, including significantly activating type I interferon signaling pathway, regulating cytokine and chemokine signaling pathway. Especially genes involved in cellular communication were significantly highly expressed post-infection.

Conclusions: All these results suggested that the interactions among immune cells played a crucial role in endothelial cell injury and immune cell recruitment after influenza virus infection. This lung-on-chip infection model combined with single-cell RNA sequencing provided a unique platform that can closely investigate the lung immune response to influenza A virus infection and new therapeutic strategies for influenza.

Keywords: lung-on-chip; influenza A virus; epithelial/endothelial barrier; immune cells; single-cell RNA sequencing

Introduction

Influenza is an acute viral respiratory illness caused by influenza virus that spreads worldwide and infects the respiratory tract. Influenza is highly contagious, characterized by sudden onset of fever, cough, chills or sweats, myalgia, and discomfort [1]. It can cause complications, like respiratory complications which can lead to pulmonary inflammation and acute lung injury, acute respiratory distress syndrome, sepsis and multi-organ failure [2]. The mortality rate of influenza infection is significantly higher in people with lung disease. Influenza-triggered epidemics cause 3–5 million cases of severe illness each year and up to 650,000 deaths annually worldwide [3]. Seasonal influenza A virus is the most common cause of infection in humans [4], causing an overall incidence of acute respiratory distress syndrome of approximately 2.7 cases per 100,000 people per year [5], accounting for approximately 4% of all hospitalizations for respiratory failure.

Airway and alveolar epithelial cells are the primary targets of the influenza A virus, causing fluid and protein leakage into the airway and alveolar lumen, through damage to epithelial cells, resulting in ventilation and air exchange dysfunction [6,7]. Clinically, many cases of severe influenza A virus infection become progressive respiratory

failure, leading to death due to diffuse alveolar damage [8], inflammation, and hypoxic respiratory failure [9,10]. Influenza virus damage to the airway, alveolar epithelium, and endothelium is caused by a combination of pathogenic and host immune responses:

(1) The inherent pathogenicity of the virus, which can be attributed to its tropism for host airway and alveolar epithelial cells;

(2) A strong host innate immune response, which although contributing to viral clearance, can exacerbate the severity of lung injury [11,12].

Influenza virus infection activates vascular endothelial cells, leading to abnormal coagulation pathways and causing vascular leakage and diffuse intravascular coagulation [13], further promoting inflammatory injury. Although the infection and pathogenic mechanisms of the influenza virus are well reported, the exact immune mechanisms and critical regulators involved in the control and clearance of the influenza virus, by the host, are yet to be identified.

Single-cell RNA sequencing (scRNA-seq) is a powerful technology for whole transcript amplification and high-throughput sequencing of single cells, which can accurately present the differences in gene expression between different cells and discover different cell subpopulations and related information [14]. Compared with traditional transcriptome sequencing technology, scRNA-seq can discover new cell types and reveal cell lineages, cell developmental trajectories, cell functions, and cell subpopulations [15]. It is widely used in many fields of life science and medical research. In particular, it enables unbiased high-throughput studies with minimal sample starting volume. It is influential in dissecting immune responses to globally reveal the complex immune response between viral and host responses after infection. For example, using scRNA-seq and cluster analysis, Steuerman *et al*. [16] revealed that the content of viral messenger RNA (mRNA) of influenza virus in epithelial cells was significantly higher than that of other cell types. The higher viral load presented a greater possibility of the virus colonizing and spreading between epithelial cells [16]. Furthermore, a study aiming to understand B cell immunity against an influenza vaccine by scRNA-seq showed that vaccination activated a fraction of peripheral memory B cells. In contrast, other memory B cells remained inactive. Expression differences in 172 genes were found between activated and inactivate memory B cells, revealing the signaling pathways relevant to the host defense against the influenza virus [17]. Therefore, single-cell studies of the influenza A virus provided important cellular and molecular insights. However, limited by the inadequacy of *ex vivo* infection models, such studies tended to mainly focus on isolated cell types and failed to depict the interactions between different types of immune cells necessary for antiviral responses [18,19], such as the interactions between lung epithelial cells, macrophages, and vascular endothelial cells, which constitute the immune microenvironment of the lung, and their effects on pulmonary capillary contents after the onset of infection.

So far, most models for studying microbial infections in the lung were mainly cellular models such as experimental animal models [20,21], organoids [22,23], and cell lines. Animal models are complex to truly mimic human pathogenesis, due to marked differences in anatomy and physiology and genetic background [24,25], especially in the composition of innate and acquired immune cells [26,27]. Most animal models can only use endpoint assays, which is challenging for exploring the mechanisms of disease development at the cellular level. A common problem with both organoid and single-cell lines is that neither enables co-culture of pulmonary capillary cells to observe the dynamics of vascular inflammation caused by pathogenic microbial infection [28]. Alveolar lavage fluid and peripheral blood samples from patients do not allow direct access to pathophysiological information about the infection and only provide a limited indirect reflection of the specific stages of disease development. Therefore, there is a need to develop new disease models that can more realistically address the pathophysiological features of human lung organs, to enhance the study of pathogenic microbial infections in the lung.

As a bionic device based on a microfluidic chip and combining multidisciplinary technologies of biology, the lung-on-chip model is equipped to simulate the complex structure and physiological functions of the lung microenvironment [29,30]. For example, the air-fluid interface composed of alveolar macrophage-alveolar epithelial cells together and the airway/alveolar epithelial cells alveolar-capillary interface by inoculating human-derived cells [31–33]. The physiological changes of lung organs can be dynamically observed at the cellular level. In addition, the lung-on-chip is made of polydimethylsiloxane (PDMS) [34], which provides a sterile surface for cell attachment [35], and also has good optical properties to support high-intensity 3D imaging and 3D imaging and analysis to help study immune cell infiltration, migration, altered vascular permeability and lung epithelial or vascular endothelial damage mechanisms in different phenotypes under viral infection [36,37]. It has unique advantages and irreplaceable research value compared with other research tools [38]. It is gradually becoming an ideal model for studying the pathogenesis, early disease warning, and intervention treatment related to lung injury by pathogenic microorganisms in the lung [39]. For example, Zhang *et al*. [40] built a lung-on-chip as a model for studying severe acute respiratory syndrome coronavirus 2 (SARS-CoV-2) infection. Furthermore, previous studies successfully applied lung-on-chip to study respiratory diseases like asthma and edema [41,42].

In this study, a human lung-on-chip model consisting of alveolar epithelial cells, vascular endothelial cells, alveolar macrophages, and perfused Peripheral Blood Mononuclear Cells (PBMCs) was constructed for simulation of the

influenza A virus infection process. The transcriptome characteristics of PBMCs after influenza A virus infection were analyzed by a single-cell RNA sequencing system. This study provides an effective microsystem platform for the organ immune response of human lung organs after an influenza A virus infection, and provides new basic research information for investigating the pathogenesis of influenza patients and the development of precise individualized immunomodulatory therapies.

Materials and Methods

Composition of the Human Lung-on-Chip Model

Lung-on-chip model made of polydimethylsiloxane (PDMS) was obtained from BEOnChip (Zaragoza, Spain). Lung-on-chip model comprises overlapping upper and lower microfluidic ducts (the overlapping parts' length, width, and height are 2.8 cm, 1 mm, and 375 µm, respectively). A 10-µm-thick polyethylene terephthalate (PET) porous membrane separates the upper and lower ducts with an 8-µm pore size, constructed as a tissue-tissue interface layer. The lung-on-chip model was thoroughly washed with PBS (phosphate-buffered saline) (Solarbio, Beijing, China). The upper and lower microfluidic channels were coated with collagen (Matrigel Matrix, Corning, NY, USA) and implanted with human lung epithelial cell line NCI-H441 cells (EK-Bioscience Biotechnology, Shanghai, China) and human peripheral blood monocyte-derived macrophages to form a continuous and complete lung epithelial layer. The lung-on-chip was incubated on a perfusion shaker set at an angle of 7° for culture, and the perfusion shaker (Mimetas, Leiden, Netherlands) was shaken every 8 min. The lower microfluidic channel was implanted with vascular endothelial cells, which were cultured for several days after perfusion to form a duct-like adnexal growth to mimic the endothelial structure of lung capillaries.

Cell Inoculation and Culture

Human alveolar epithelial cell line NCI-H441 was cultured in RPMI-1640 medium (Gibco, Grand Island, CA, USA) supplemented with 10% fetal bovine serum (FBS) (Gibco, Grand Island, CA, USA) and 1% Penicillin-Streptomycin (P/S) (Gibco, Grand Island, CA, USA). Human umbilical vein endothelial cells (HUVECs, iCell Bioscience Inc, Shanghai, China) were cultured in an Endothelial Cell Medium (ECM, ScienCell, Carlsbad, CA, USA) supplemented with 5% FBS, 1% Endothelial Cell Growth Supplement (ECGs, ScienCell, Carlsbad, CA, USA), and 1% Penicillin-Streptomycin. HUVECs 2×10^5 inoculate in the lower channel of the chip. All cells were validated through STR testing, and tested for mycoplasma, using mycoplasma detection kit (Meilune, Dalian, China). After the cells adhere to the wall, the chip is incubated on a 7° perfusion shaker at 37 °C and 5% CO_2. After three days, 2×10^5 NCI-H441 cells were inoculated into the upper channel, and the culture medium was changed daily. After six days, macrophages derived from human peripheral blood mononuclear cells (PBMCs, Milestone Biological Science & Technology Co., Ltd., Shanghai, China) were inoculated on the chip. The number was 1/10 of that of epithelial cells. Influenza A virus infection was carried out after seven days. After 48 hours of infection, RPMI-1640 culture medium was used with PBMCs infused with 2×10^5/mL density, and the chips were incubated on a 7° perfusion shaker at 37 °C and 5% CO_2 for 24 hours.

Infection of Lung-on-Chip Model with Influenza Virus

Influenza A virus strain A/Puerto Rico/08/1934 was obtained from CAS Key Laboratory of Animal Ecology and Conservation Biology, Institute of Zoology, Chinese Academy of Sciences, Beijing, China, and propagated in Madin-Darby canine kidney cells (MDCK, Procell, Wuhan, China). The human lung-on-chip model has infected with the influenza A virus (MOI 1) in NCI-H441 cells under static conditions seven days after perfusion. The cells were co-incubated with influenza A virus for 1 hour, then rinsed with PBS and replaced with fresh medium.

Macrophage Differentiation

100 µL of 5 µg/mL Human Recombinant M-CSF (STEMCELL, Vancouver, Canada) were added to 10 mL of ImmunoCult™-SF Macrophage Medium (STEMCELL, Vancouver, Canada) (final concentration 50 ng/mL). This was followed by adding monocytes (Milestone Biological Science & Technology Co., Ltd., Shanghai, China), at a concentration of 1×10^6 cells/mL, to 5 mL of ImmunoCult™-SF Macrophage Differentiation Medium (ImmunoCult™-SF Macrophage Medium + Human Recombinant M-CSF), and the cell suspension was added to a 6-well plate (Nest, Wuxi, China), which was incubated at 37 °C for four days. After that, 2.5 mL (half of the original volume) of fresh ImmunoCult™-SF Macrophage Differentiation Medium were added to the culture plate on day 4. Subsequently, the supernatant was removed from the culture dish, to a 15 mL centrifuge tube on day 6, and centrifuged at 300 ×g for 10 minutes. The supernatant then was removed, and the cell pellet was retained. 5 mL of PBS and 0.5% bovine serum albumin (BSA, Beyotime, Beijing, China) were added to the culture dish and the cells were aspirated up and down several times, with a pipette. The cell suspension was transferred to a centrifuge tube containing the cell pellet. The tube was centrifuged at 300 ×g for 10 minutes. After the supernatant was removed and discarded, the macrophages were collated and resuspended in the epithelial cell medium, then counted and grown into the lung chip upper channel.

Analysis of Cytokines in Lung-on-Chip Supernatants by Using Multiplex Bead Immunoassay

Infection time 0 was set as one hour after the influenza A virus infection. The upper and lower channel supernatant of the chip was collected at the time point of the 12th hour after infection and stored in the refrigerator at –80 °C. 100 µL supernatant was taken for protein concentration identification of the total protein concentration of the supernatant, using the Bradford method. The rest of the samples were detected using the cell multi-factor detection kit in the supernatant through the liquid-phase microsphere suspension chip system (Bio-Plex Pro Human Cytokine Screening Panel, 48-Plex, Bio-Joy Biotechnology Co., Shanghai, China).

Permeability Assay

To assay the permeability of the epithelial and endothelial barriers, 1 mg/mL of 3–5 kDa fluorescein isothiocyanate (FITC)-dextran (Sigma-Aldrich, Schnelldorf, Germany) in phenol red-free DMEM/F12 medium (Gibco, Grand Island, CA, USA) was injected into the upper chamber of the chip. The alveolar models were incubated for 1 h under static conditions. Subsequently, the media from the lower and upper chambers were collected and the fluorescence intensity (ex. 490 nm; em. 520 nm) was measured, using a Tecan Infinite M200 Pro microplate reader (Tecan Group Ltd., Maennedorf, Switzerland). The permeability coefficient (Papp) was calculated according to Papp (cm s^{-1}) = (dQ/dt)(1/AC_0). Where dQ/dt represents the steady-state flux (g s^{-1}), A is the culture surface area (cm^2), and C_0 is the initial concentration (mg mL^{-1}) [43].

Immunofluorescence Staining

In lung-on-chip immunofluorescence imaging, cells were washed via upper and lower channels using PBS; the microarray was fixed with 4% paraformaldehyde for 15 minutes at room temperature. They were then washed three times with PBS, and treated with 0.1% Triton for 10 minutes at room temperature, after washing three times with PBS again, they were finally closed with 5% BSA for 1 hour at room temperature. Lung-on-chip was used with antibodies to surfactant protein A (SP-A) (1:1000, NOVUS, Littleton, CO, USA), F-actin (1:500, Beyotime, Beijing, China), Zona occludens 1 (ZO-1) (1:1000, Abcam, Cambridge, MA, USA), E-Cadherin (1:1000, Proteintech, Wuhan, China), VE-Cadherin (1:1000, Proteintech, Wuhan, China), CD68 (1:1000, Proteintech, Wuhan, China), DAPI (4′,6-diamide-2-phenylindol) (Beyotime, Beijing, China), and H1N1 protein (Bioss, Beijing, China) to visualize lung surface active protein A, F-Actin, macrophage markers, tight junction proteins, nuclei, and influenza A virus. Samples were closed and stained against the primary antibody (1:100–200) at room temperature for 1 h. After washing three times with PBS, the goat anti-rabbit IgG secondary antibody (Abcam, Cambridge, UK) was added at a dilution of 1:800 and incubated for 40 min at room temperature. The samples were washed three times in PBS and stained in an anti-fluorescence quencher. Fluorescence imaging was performed by confocal microscopy (Olympus, Hamburg, Germany).

10× Genomics Single-Cell Sequencing

PBMCs perfused from the lower tract of the lung chip in each experimental group were aspirated and washed twice with PBS for subsequent experiments. Cells were resuspended in PBS and incubated with magnetic suspension beads (QDSphere, Beijing, China) to exclude dead cells. Afterwards, cells were suspended in PBS containing 0.04% BSA and passed through a 70 mm cell filter (Thermo Scientific, Waltham, MA, USA) and counted with a Luna™ automated cell counter (Logos Biosystems, Anyang-si, South Korea). After cell counting adjustments, 30,000 cells were loaded into Chromium™ controllers for splitting single cells into nanoliter gel bead emulsions (GEMs). Single Cell 3′ Reagent Kits v3 were used for reverse transcription, complementary DNA (cDNA) amplification and gene epitope library construction following the detailed protocols provided by 10× Genomics (Chromium Single Cell 3′ Reagent Kits v3, Pleasanton, CA, USA). Se-quencing was performed using a Hiseq XTen PE150 sequencer (Illumina, San Diego, CA, USA).

Single-Cell RNA-seq Data Processing and Analysis

Raw sequencing data were first quality checked with FastQC and then trimmed with FASTX-Toolkit 0.0.13 (Cold Spring Harbor Laboratory, Cold Spring Harbor, NY, USA). Gene counts were calculated by comparing fastq reads to the human GRCh38 genome using CellRanger 4.0.0 (10× Genomics, Pleasanton, CA, USA). Single-cell clusters were annotated by their signature genes in the Loupe Browser (10× Genomics). Unique molecular identifiers (UMIs) belonging to single-cell clusters were isolated and further analyzed by Seurat 4.3.0 (New York University, New York, NY, USA). Inferior cells and twins were removed according to the following criteria based on the number of UMIs and the percentage of mitochondrial genes: Genes expressed in <3 cells; >200 genes in a cell; $>15\%$ of mitochondrial genes; and $>18{,}000$ genes per cell or <50 genes. Variable genes were calculated using the Seurat function “FindVariableGenes” as per the following criteria: Cutoff values from 0.01 to 10 for x and 0.5 for y. A total of 3000 variable genes were imported into the Seurat “RunPCA” pipeline. The Seurat function “FindClusters” was used to find clusters with a resolution of 0.5. The scaled data is used to plot the heat map and the normalized data is used to plot the violin map. For the feature maps, the normalized data are plotted as pot-bottom colors on the scatter plots of tSNE_1 and tSNE_2. After excluding low

quality cells and erythrocytes, we processed and integrated the scRNA-seq data to generate single-cell gene information for 93,146 cells, with an average of 11,643 cells per sample.

Differential Gene Expression Analysis

Differential gene expression analysis was performed using the FindMarkers function of Seurat 4.3.0 (New York University, New York, NY, USA). Gene expression with an absolute value of fold change of not less than 2 and an ad-adjusted *p* value of less than 0.05 was defined as significantly differentially expressed genes (DEGs).

GO Enrichment Analysis

Significant differences between different clusters were abstracted as up- and down-regulated genes and reordered by GO (Gene Ontology) enrichment analysis using clusterProfiler V4.2.2 (Roswell Park comprehensive cancer center, Buffalo, NY, USA). The top 15 related biological process genes were determined.

Gene Set Enrichment Analysis

Genome enrichment analysis was performed with microarrays generated by GSEA V4.1.0 (Broad Institute, Cambridge, MA, USA). The Hallmark gene set and the Kyoto Encyclopedia of Genes and Genomes (KEGG) gene set were selected for analysis. Gene sets that met the normalized enrichment score (NES) >1, p-value < 0.05 and false discovery rate (FDR) q-value < 0.25 were removed as significantly enriched gene sets.

Cell–Cell Communication Analysis

To be able to systematically analyze cell-cell communication molecules, cell communication analysis was carried out based on CellPhoneDB [44], a public repository of ligands and receptors and their interactions. Membrane secretory and peripheral proteins were annotated for clusters at different time points. Significant means and cellular communication significance (p-value < 0.05) were calculated, based on the normalized cellular matrix achieved by interaction and Seurat normalization.

Image Analysis and Quantification

Cytometric quantification analysis was performed using iMaris x64 9.0.1 software (Oxford instruments, Oxford, UK). The number of recruited PBMCs was calculated using iMaris x64 9.0.1 software (Oxford instruments, Oxford, UK) by Z-axis analysis.

Statistical Analysis

Statistical differences were analyzed by Student's t-test between every two groups and one-way analysis of variance (ANOVA) for multiple groups. The values where $p < 0.05$ were taken as being statistically significant. Statistical data analysis was performed using GraphPad Prism software (version 9.0.2, GraphPad Software, Inc., San Diego, CA, USA).

Results

Characterization of Human Lung-on-Chip

The lung-on-chip consists of overlapping upper and lower microfluidic ducts (the length, width and height of the overlapping parts are 2.8 cm, 1 mm, and 375 µm, respectively). The upper and lower ducts are separated by a porous membrane with a thickness of 10 µm and a pore size of 8 µm, allowing the adhesion, migration, crossing, and recruitment of immune cells caused by viral or bacterial infections. An inlet and outlet for perfusion are provided outside the lung-on-chip, corresponding to the upper and lower ducts, to facilitate pipette operation for cell injection, perfusion, pathogenic microbial infestation, washing, and aspiration. In addition, the presence of uniformly distributed tiny pores on the porous membrane allows the passage of PBMCs, based on which the structure can simulate the phenomenon of immune cells being recruited in the peripheral blood after pathogen invasion of the lung (Fig. 1).

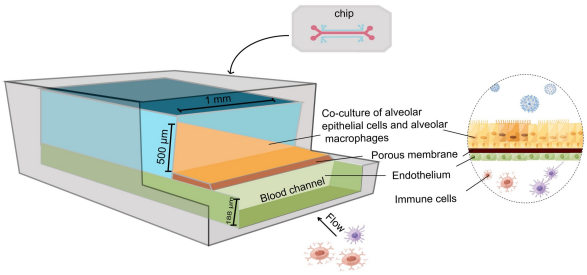

Fig. 1. Schematic diagram of the lung chip.

For use, the upper and lower microfluidic tracts were coated with collagen (Matrigel Matrix) and implanted with human lung epithelial cell line NCI-H441 cells and human peripheral blood monocyte-derived macrophages, to form a continuous and complete lung epithelial layer. The lower microfluidic tract was implanted with vascular endothelial cells, which were cultured for several days after perfusion to form a duct-like wall to mimic the capillary endothelium of the lung structure. PBMCs were then added to the lower channel for continuous perfusion. A co-culture lung and vascular endothelial cells on lung-on-chip was carried out for up to 7 days. Confocal micrographs showed that co-culture could form an intact lung epithelial and vascular layer (Fig. 2A–D). Both lung epithelial and vascular endothelial cells commonly expressed functional markers (ZO-1 and VE-Cadherin) (Fig. 2D–I), as well as expression of the macrophage marker CD68 (**Supplementary Fig. 1**), and immunofluorescence staining visualized the interface

between the epithelial and endothelial layers (Fig. 2J), constructing lung-on-chip with ideal z-axis resolution to distinguish between the epithelial and endothelial cell layers. The expression of the epithelial cell marker E-cadherin (**Supplementary Fig. 2**) and the alveolar type II epithelial marker SP-A (**Supplementary Fig. 3**) were detected. These results indicated that NCI-H441 cells were similar to human primary alveolar epithelial cells. The human alveolar microarray could therefore be used to mimic the physiological barrier of alveolar capillaries.

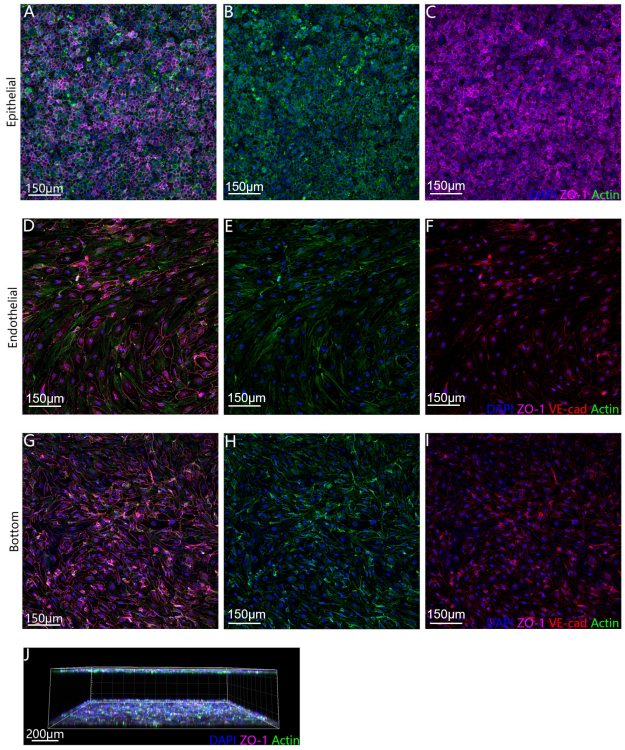

Fig. 2. Lung epithelial cells are co-cultured with vascular endothelial cells on lung-on-chip. (A–C) Marker expression of the epithelial cell layer of the human lung-on-a-chip model. Expression of epithelial markers zonula Occludens-1 (ZO-1) (purple) and actin (green) was confirmed by immunofluorescence staining. (D–I) Marker expression of the endothelial cell layer of the human lung-on-a-chip model. Expression of endothelial markers VE-cadherin (red) and actin (green), as confirmed by immunofluorescence staining. (J) Lateral view of the interface between the pulmonary epithelium and the vascular endothelium. Nuclei were stained with 4′,6-diamide-2-phenylindol (DAPI) in blue. The scale bar represents 150 μm and 200 μm. N = 3.

Influenza A Virus Infiltrates the Epithelial Layer of the Lung-on-Chip

To simulate the infection of the influenza A virus in the alveoli, we inoculated the influenza A virus with MOI of 1 into the upper lung chip channel for 1 h. Subsequently, the culture medium was changed, and immunofluorescence staining was performed after 24 h of infestation, followed by confocal microscopic photography. Infection did not cause changes in the integrity of the epithelial layer (Fig. 3A–F). In addition, cell counting by immunofluorescence quantification of nuclei (DAPI) (Fig. 3G) showed that the number of epithelial cells did not change significantly after influenza A virus infection compared with the control group. In contrast, quantification of the tight junction protein ZO-1 by fluorescence area and total fluorescence intensity showed no significant change in the tight junction degree of the epithelial layer, indicating that infection of the epithelial layer does not lead to a significant difference in the integrity of the epithelium ($p > 0.05$) (Fig. 3H,I).

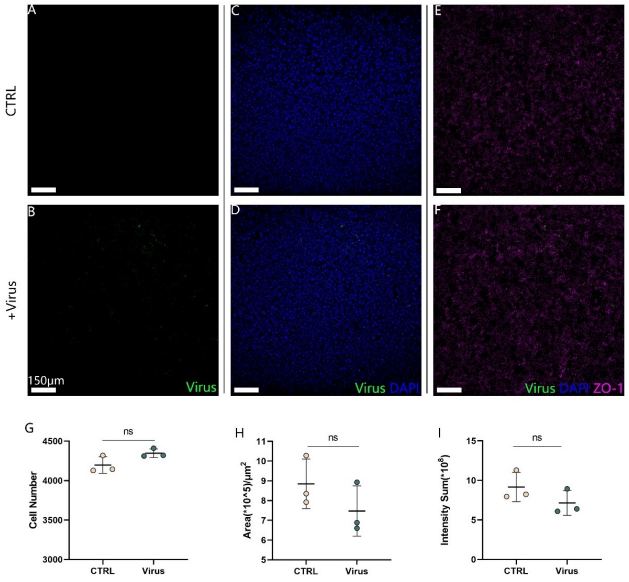

Fig. 3. Influenza A virus infection of the epithelial layer of the lung chip. (A–F) Immunofluorescence staining of the epithelial layer for ZO-1 (purple) is shown for the CTRL group and influenza A virus-infected group. The scale bar is 150 μm. (G) Cell counting by immunofluorescence quantitative cell nuclei (DAPI). (H,I) Quantification of viral amplification by fluorescence area and total fluorescence intensity, respectively. The scale bar represents 150 μm. Data information: Data are shown as mean ± standard deviation (SD) [n = 6 in (G) to (I)]. ns represents $p \geq 0.05$. N = 3.

Immune Response to Human Lung-on-Chip after Influenza A Virus Infection

To analyze the integrity of the whole biochip system, permeability assays were carried out using FITC-dextran, to verify the integrity of the endothelial and epithelial cell layers by detecting fluorescence. The integrity of vascular endothelial cells was significantly disrupted by immunofluorescence cell counting of vascular endothelial cells compared with the control group ($p < 0.05$) (Fig. 4A). It was

able to show that influenza A virus infection significantly reduced the barrier function compared to the mock-treated chamber ($p < 0.001$) (Fig. 4B).

Significantly, more PBMCs appeared on the epithelial and endothelial dividing surfaces of the organ chips after influenza A infection, indicating that influenza A virus infection induced an immune response resulting in the recruitment of PBMCs under the vascular layer and adhesion to the dividing interface between endothelial and epithelial cells under perfusion conditions ($p < 0.001$) (Fig. 4C–F).

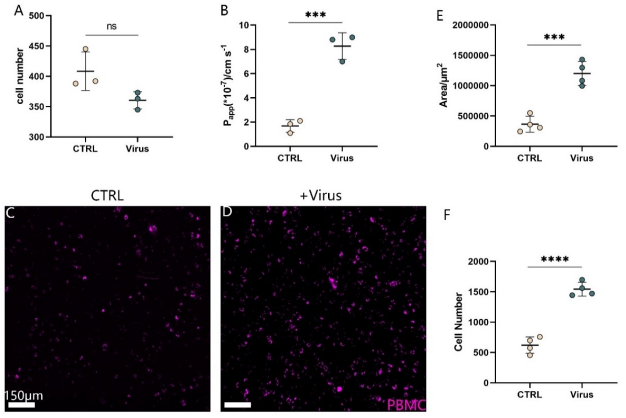

Fig. 4. Disruption of endothelial layer barrier function and recruitment of peripheral blood mononuclear cells (PBMCs) after influenza A virus infection. (A) Endothelial cell count after influenza A virus infection. (B) Barrier function in human lung-on-chip model. (C,D) Recruitment of PBMCs after influenza A virus infection in lung-on-chip. (E,F) Quantification of PBMCs recruitment by fluorescence area and cell counts, respectively. Data information: Data are shown as mean ± standard deviation (SD) [n = 6 in (E) to (F)]. The scale bar represents 150 μm. Data are representative of at least three independent experiments. The bars represent the mean value, the solid line represents the median value, and the error bars represent the standard deviation. ns represents $p \geq 0.05$, *** represents $p \leq 0.001$, and **** represents $p \leq 0.0001$.

Changes of Inflammatory Factor Levels in Influenza A Virus Infection

To explore the differences in inflammatory responses in the epithelial and endothelial cell layers following influenza A virus infection, multiple cytokines were tested, to determine pro- and anti-inflammatory responses. Influenza A virus infection group led to more significant production of pro-inflammatory factors interleukin-1β (IL-1β), IL-6, and interferon-γ (IFN-γ), as well as chemokines CCL3 and CLL5 compared to the uninfected group (Fig. 5).

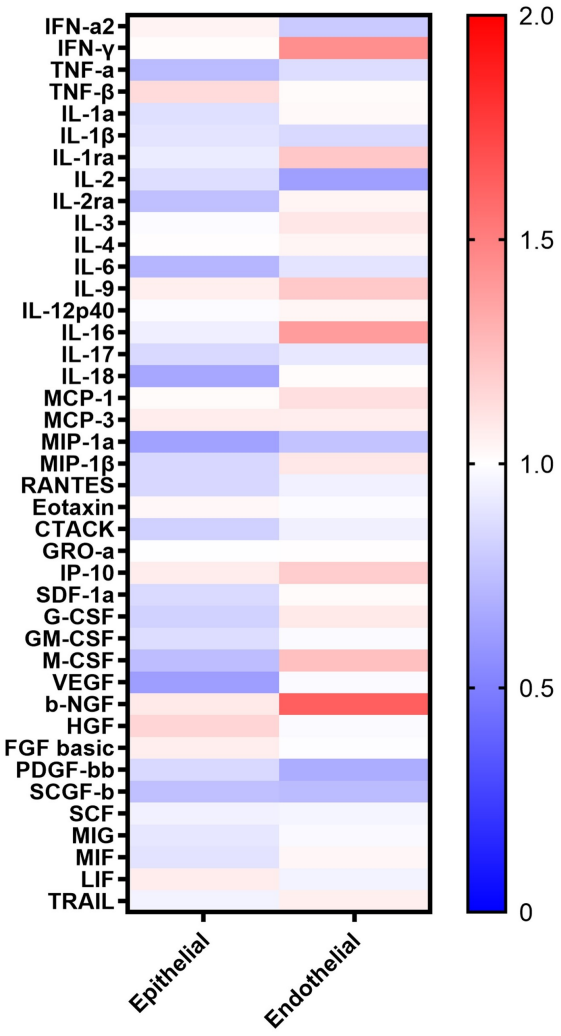

Fig. 5. Cytokine secretion on the epithelial and endothelial side after infection with influenza virus. A ratio greater than 1 indicates an increase in the cytokine expression level, and a ratio less than 1 indicates a decrease in the cytokine expression level. Data information: The bars represent the mean value, and the solid line represents the median value.

Immune Profiling of PBMCs after Single-Cell Transcriptome Sequencing Analysis in Influenza A Virus-Infested Lung-on-Chip

To explore the immune characteristics of PBMCs after influenza A virus infection of the lung-on-chip, single-cell transcriptome sequencing analysis of PBMCs after influenza A virus infection of the lung chip and in the uninfected lung-on-chip subchannel was performed. Seven clusters were identified and classified into five major immune cell groups: B lymphocytes, cluster of differentiation 4 (CD4) T lymphocytes, CD8 T cells, natural killer (NK) cells, and monocytes (Fig. 6A). The percentage of each im-

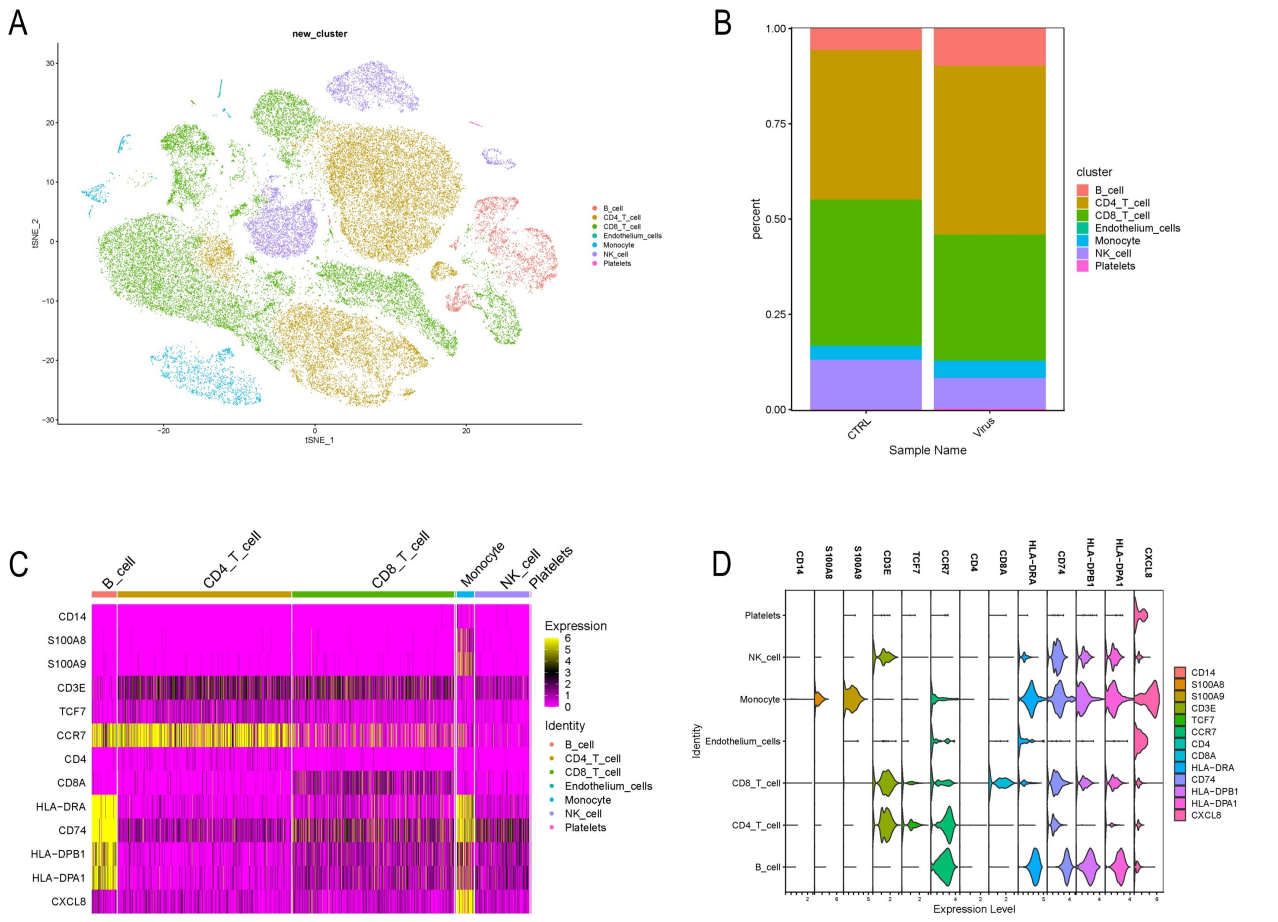

Fig. 6. Cell composition of PBMCs in the lung microarray and control groups infected with influenza A virus. (A) tSNE representation of the immune cell populations identified in the single-cell RNA sequencing (scRNA-seq) data. Data from all four samples (two samples per group) were pooled for analysis. (B) Frequency distribution of the five cell types in the two groups. Monocytes, CD4 T cells, CD8 T cells, natural killer (NK) cells and B cells are indicated as orange, moderate mauve magenta, indistinct rose, blue and brick red, respectively. (C) Heat map of gene expression for the five major immune cell subsets. Highly expressed representative genes are listed next to each other. Relative expression levels are defined from 6 to 0, and colors range from yellow to purple. The higher the gene expression, the more yellow the color. (D) Expression of representative genes in each subpopulation is presented as a violin plot.3.6. Immune Features of B Cells after Influenza A virus infection.

mune cell in both groups was also determined (Fig. 6B), where the percentage of B cells and CD4 T cells was significantly higher in influenza A virus-infected group compared to the control group. Heat maps were generated based on the top 20 genes of each cluster (Fig. 6C), while characteristic genes were listed to show the overall view of these immune cells (Fig. 6D). The results of the percentage of immune cells in each group in single-cell RNA showed that the percentage of B cells and CD4 T cells were significantly higher in the influenza A virus-infected group compared with the control group (Fig. 6B), suggesting an immune disorder in influenza A virus-infected group, while B cells and CD4 T cells played important immune roles in all periods of viral infection, so we focused on resolving the immune characteristics of B cells and CD4 T cells in influenza A virus-infected and control groups by single-cell RNA sequencing in the subsequent study.

Based on the results of single-cell RNA sequencing, the differentially expressed genes of B cells in influenza A virus-infected and control groups were compared. Compared with B cells in the control group, that in influenza A virus infection expressed a significantly larger number of interferon-inducible genes, such as *IFITM1* and *IFITM3*, inflammation-related genes (*JUND*, *MIF*) and chemokines (*CCL3*, *CCL5* and *CXCL10*), which play an important role in the inflammatory response and type I interferon response (Fig. 7A). Kyoto Encyclopedia of Genes and Genomes (KEGG) enrichment analysis showed that B cells were enriched in genes related to cytokine-receptor interactions, Janus kinase-signal transducer and activator of transcrip-

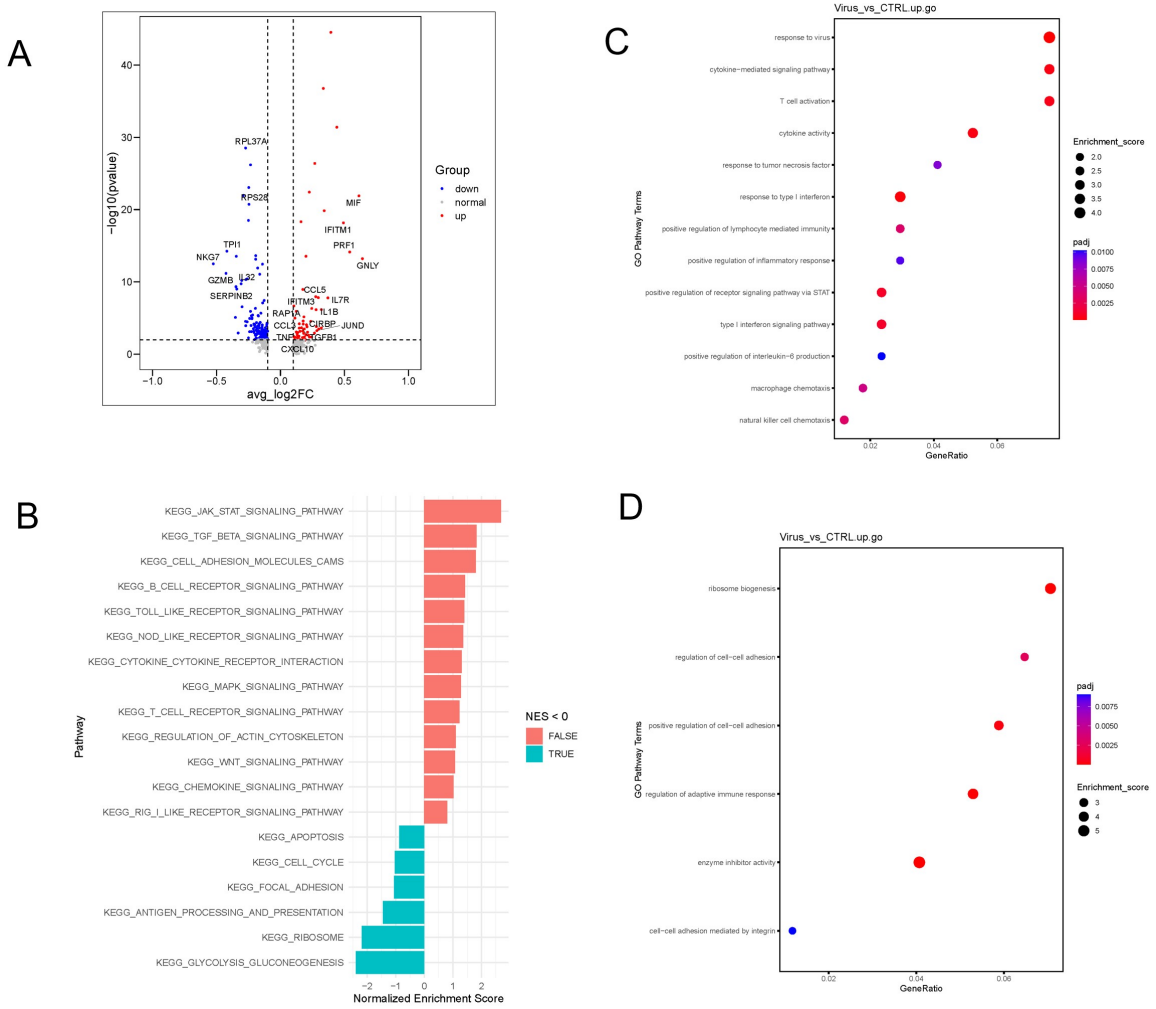

Fig. 7. Characterization of B cells in influenza A virus infection. (A) Volcano plots of B cells of influenza A virus-infected group versus B cells of uninfected group, red represents upregulation and blue represents downregulation. (B) Kyoto Encyclopedia of Genes and Genomes (KEGG) pathway analysis between B cells of the influenza A virus-infected group and B cells of the uninfected group. (C,D) GO analysis with genes highly expressed and lowly expressed in the influenza A virus-infected group compared with the uninfected group.

tion (JAK-STAT) signaling pathway, and chemokine signaling pathway (Fig. 7B). Gene Ontology (GO) enrichment analysis was carried out on B cells to identify biological processes significantly regulating gene enrichment (Fig. 7C,D). In summary, genes related to type I interferon signaling pathway, viral response, and cellular chemotaxis were actively expressed in influenza A virus infection.

Immune Features of CD4 T Cells after Influenza A Virus Infection

Based on the results of single-cell RNA sequencing, the differentially expressed genes of T cells in influenza A virus-infected and control groups were compared. Compared with CD4 T cells in the control group, that in influenza A disease infection expressed a significantly larger number of *IFITM2* interferon-inducible genes, inflammation-related genes (*JUND*, *GNLY*), and chemokines (*CCL2*, *CCL3*, *CCL4*, *CCL5* and *CXCL8*), which play an essential role in the inflammatory response and type I interferon response (Fig. 8A). KEGG enrichment analysis showed that CD4 T cells were enriched for TOLL-like receptor signaling pathways, cytokine-receptor interactions, and chemokine signaling pathways (Fig. 8B). GO analysis on CD4 T cells was carried out. Influenza A virus infection induced various innate immune and antiviral responses, including defense responses to viruses, type I interferon signaling pathways, and cytokine regulatory signaling pathways (Fig. 8C,D). The immune response of CD4 T cells activated in the early stages of influenza A virus infection is highly inflammatory.

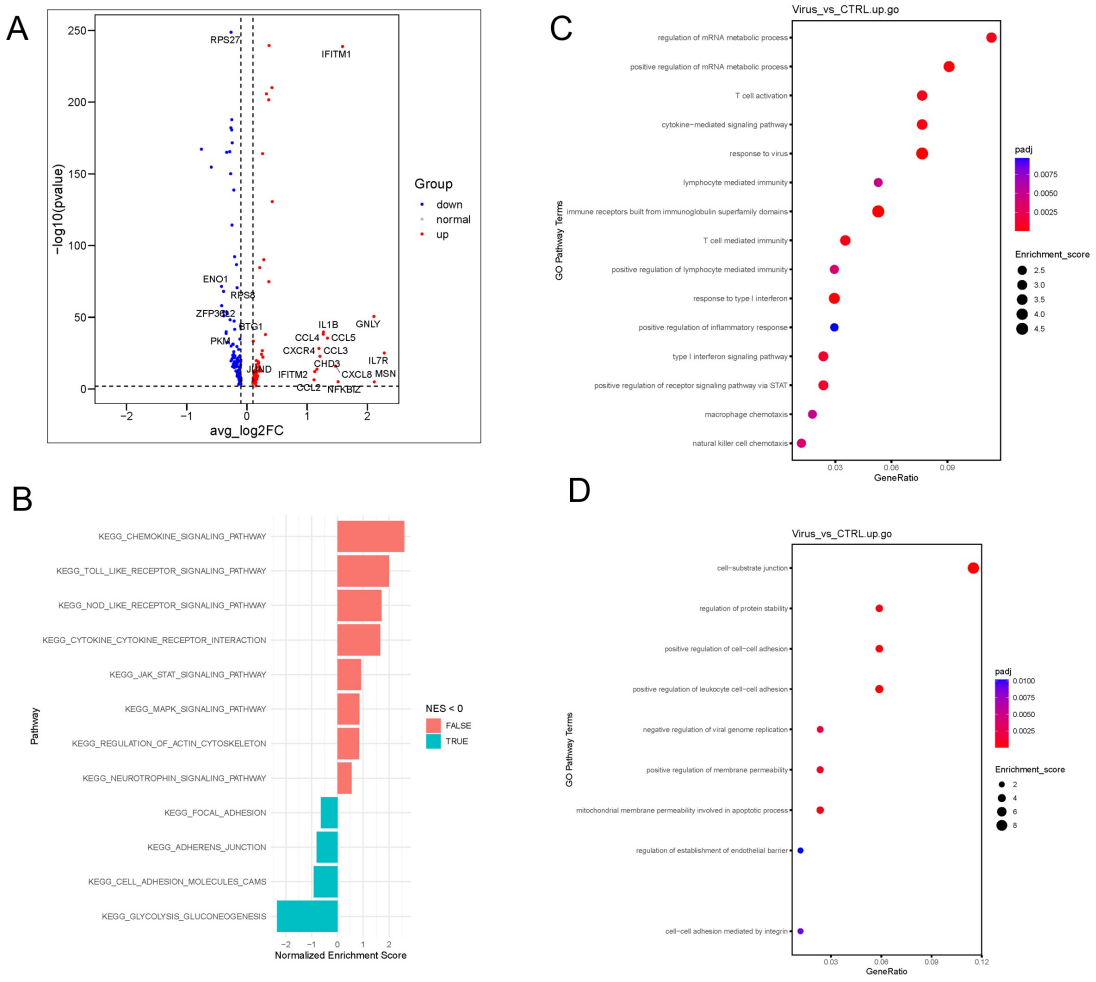

Fig. 8. Characterization of CD4 T cells in influenza A virus infection. (A) Volcano plots of CD4 T cells of influenza A virus-infected group versus CD4 T cells of uninfected group, red represents upregulation and blue represents downregulation. (B) KEGG pathway analysis between CD4 T cells of the influenza A virus-infected group and CD4 T cells of the uninfected group. (C,D) GO analysis with genes highly expressed and lowly expressed in the influenza A virus-infected group, compared with the uninfected group.

Cell-Cell Communication of Immune Cells between Influenza A Virus-Infected and Control Groups

Since comparing differentially expressed genes may not reflect signaling networks through soluble and membrane-bound factors, cellular communication between immune cells in influenza A virus-infected and uninfected groups was analyzed respectively, using CellPhoneDB. This method uses a comprehensive database of signaling molecular interactions, and we performed a cell-cell contact analysis. Effective mutual cellular communication between B cells and CD4 T cells was observed in both influenzas A virus-infected and control groups (Fig. 9A,B). CellPhoneDB was used to calculate the specific enrichment of ligand-receptor pairs in B and CD4 T cells and analyze the interactions between B cells and CD4 T cells in both virus-infected and control groups (Fig. 10A,B). The results of receptor-ligand specificity analysis showed that HLA-C-KIR2DL3 and CCR7-CCL19 had the most significantly vigorous communication intensity between B lymphocytes and CD4 T lymphocytes in the influenza A virus-infected group. By contrast, this was not observed in the control group, and HLA-C-KIR2DL3 acted as an antigen-presenting molecule and ligand receptors to regulate the immune system's response to infection, and CCR7-CCL19 as ligand receptors and chemokines, respectively, involved in regulating the migration and localization of immune cells. They constitute the primary communication relationship and are significantly involved in the interaction between B cells and CD4 T cells during influenza A virus infection.

In addition, cytokine signaling pathways were analyzed using CellPhoneDB, and inflammatory signaling (IL-1β, IL-6) and chemokine signaling (CCL3, CCL5) were significantly enhanced during influenza A virus infection (**Supplementary Fig. 4**), which is also consistent with our multi-factor assay results.

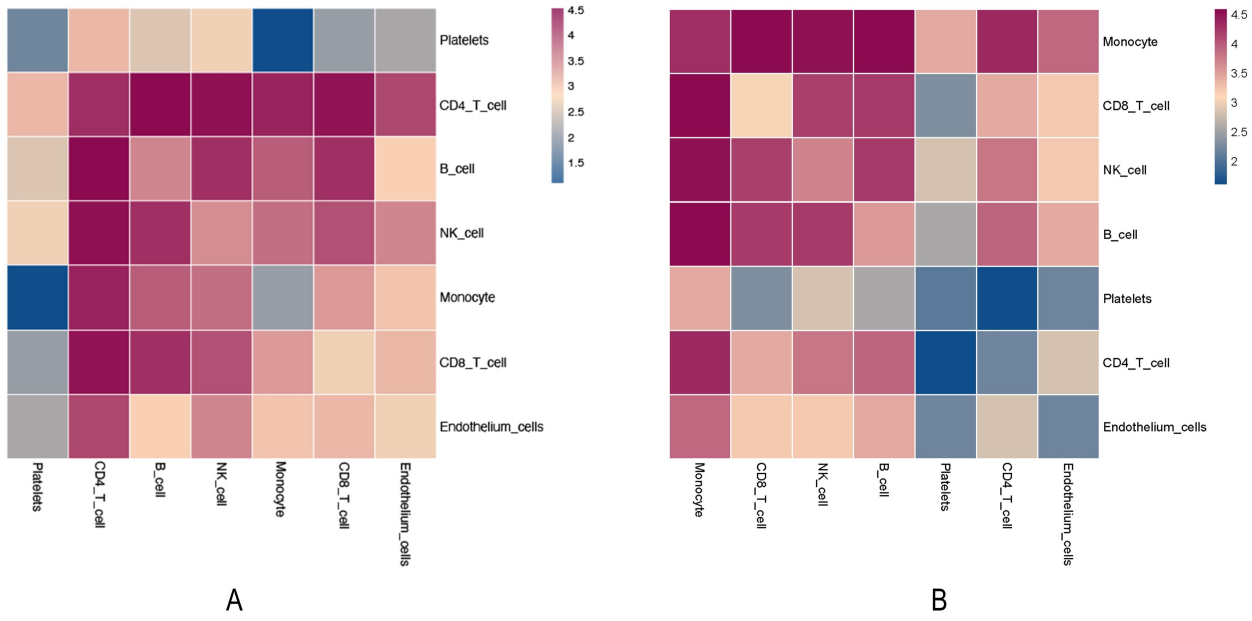

Fig. 9. The communication network of immune cells of influenza A virus-infected and influenza A virus-uninfected groups. (A) Heat map of the number of reciprocal receptor ligands of PBMCs in influenza A virus-infected group. (B) Heat map of the number of reciprocal receptor ligands of PBMCs in the uninfected group.

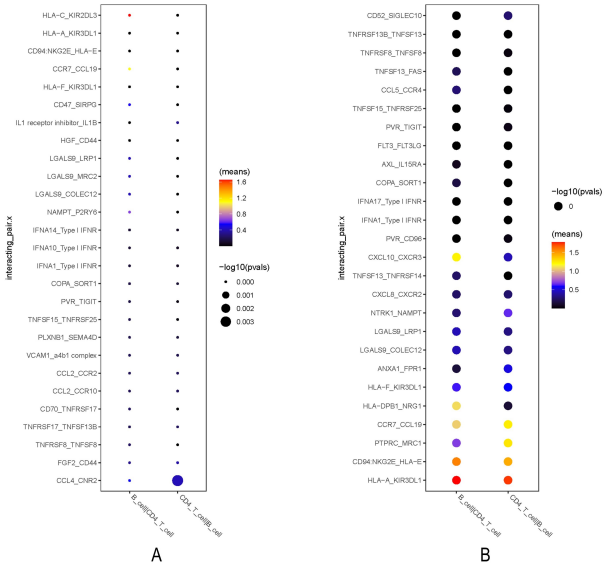

Fig. 10. Ligand receptor analysis of immune cells of influenza A virus-infected and uninfected groups. (A) Bubble diagram of receptor-ligand interaction between B cells and CD4 T cells in influenza A virus-infected group. (B) Bubble diagram of receptor-ligand interaction between B cells and CD4 T cells in the uninfected group. The dotted ones in the figure represent the significance of the *p*-value of the communication effect, and the dot's color represents the communication intensity.

Discussion

Firstly, this study constructed a vascularized lung-on-chip model of alveolar macrophage-alveolar epithelial cell-vascular endothelial cell co-culture and realized the perfusion of PBMCs within the vascularized channels. The lung-on-chip model constructed can successfully express features such as lung epithelial tight cell junction protein E-cadherin, ZO-1, and type II alveolar epithelial cell marker SP-A [45], indicating that this system successfully mimics the micro-physiological environment of human lung organs [46]. In addition, the study established a human disease model of influenza A virus infection on lung-on-chip which could reflect the pathophysiological changes and immune responses after influenza A virus infection of lung tissues, including virus invasion, cellular immune response, and immune cell recruitment in human alveolar sites.

Influenza is an important human pathogen that can cause substantial seasonal and pandemic morbidity and mortality [47]. Although influenza vaccines have been developed [48], the annual mortality rate hints at the urgency of developing novel vaccines and drugs against influenza viruses. In light of this, it remains imperative to explore the immune landscape in the lungs of influenza patients and decipher the mechanisms of how immune cells respond to viral infection. Therefore, this study collected PBMCs after influenza A virus infection of lung-on-chip and compared the functional differences, characteristics, and intercellular communication of immune cell taxa after infec-

tion by single-cell RNA sequencing. Single-cell RNA sequencing analysis showed that the proportion of B cells and CD4 T cells in the influenza A virus-infected group was significantly higher than that in the uninfected group, with 9.79% of B cells and 44.3% of CD4 T cells in the influenza A virus-infected group whereas 5.68% of B cells and 39.1% of CD4 T cells in the control group, which suggested that the balance of immune content between B cells and CD4 T cells was disturbed, and B cells and CD4 T cells played an essential immunomodulatory role in response to influenza A virus infection. Compared to the uninfected group, influenza A virus-infected group exhibited a more extensive innate immune and inflammatory response, such as a significant enrichment of type I interferon signaling pathways, cytokine regulatory signaling, and chemokine signaling pathways, as well as a significant expression of inflammation-related genes (*JUND*, *MIF*) and chemokine genes (*CCL3*, *CCL5* and *CXCL10*). A recent study reported that macrophage migration inhibitory factor (MIF) impairs immunity and increases inflammatory responses in antiviral hosts during influenza infection and suggested that targeting MIF during influenza virus infection may be a beneficial therapy [49]. The results of this study are similar to these findings and suggest that disease model of influenza virus has advantages in reflecting the human-associated immune response of the lung.

Lung-on-chip helps to uncover the intercellular communication mechanisms behind the immune response through the co-culture of immune cells in the lungs. On single-cell sequencing, the study found significantly enhanced transmission of chemokines and inflammatory signals between B cells and CD4 T cells in the influenza A virus infection group, which was further validated by measuring cytokines and chemokines in the upper and lower channels of the lung microarray in the infection group, with IL1-β, IL-6, CCL3 and CCL5 rising in the supernatant showing the signature of cytokines, and also with single-cell RNA sequencing analysis results giving us insight into consistent immune responses and communication of immune cells during influenza A virus infection. Also, on confocal microscopic photography after immunofluorescence staining of PBMCs in the lower lung chip channels, the study found that PBMCs in the endothelial layer were recruited in large numbers to the junction of the epithelial and endothelial layers of the lung-on-chip during influenza A virus infection and migrated through the porous membrane to recruit to the epithelial layer of the lung chip. Pulmonary alveolar epithelial cells are the primary target cells of influenza A virus infection [50]. Many severe influenza patients often show progressive respiratory failure and disseminated intravascular coagulation clinically [51]. Compared with the non-infected group, HLA-C-KIR2DL3 in B cells and CD4 T cells regulate the immune response of the immune system to infection as antigen-presenting molecules and ligand receptors [52], CCR7-CCL19, as ligand-receptor and chemokine, respectively, and participate in regulating the migration and localization of immune cells [53]. They constitute the primary communication relationship and significantly participate in the interaction between B cells and CD4 T cells during influenza A virus infection. These findings are highly consistent with the clinical and pathological manifestations of severe patients with influenza A virus infection.

Conclusions

The lung-on-chip model is a supplement to the animal model. This study, through the combination of the humanized lung-on-chip system and the single-cell sequencing technology system, reflected the pathophysiological changes related to the human body, the host's immune response to the virus, and the interaction between immune cells at the organ level. This research strategy based on lung-on-chip could become an ideal model for studying the pathogenesis, early disease warning, and intervention treatment of lung injury caused by pathogenic microorganisms.

Availability of Data and Materials

The original data presented in the study are available on request from the corresponding author.

Author Contributions

LX and QW conceived and designed the study; SG, PP and JW conceived the experiments; SG, YS, YZ and WG performed the analysis of the metabolomics data; FS, YC and HQ performed the investigation and collection of the background information for the enrolled subjects; SG, PP, YZ and JW were involved in editing the manuscript. All authors discussed the results and commented on the manuscript. All authors have read and agreed the final manuscript. All authors have participated sufficiently in the work and agreed to be accountable for all aspects of the work.

Ethics Approval and Consent to Participate

Not applicable.

Acknowledgment

We are grateful for Bo Guang in helping us improve the language.

Funding

This work was supported by the National Natural Science Foundation of China (Grant No.82172109).

Conflict of Interest

The authors declare no conflict of interest.

Supplementary Material

Supplementary material associated with this article can be found, in the online version, at https://doi.org/10.24976/Discov.Med.202335177.55.

References

[1] Paules C, Subbarao K. Influenza. Lancet. 2017; 390: 697–708.

[2] Javanian M, Barary M, Ghebrehewet S, Koppolu V, Vasigala V, Ebrahimpour S. A brief review of influenza virus infection. Journal of Medical Virology. 2021; 93: 4638–4646.

[3] Iuliano AD, Roguski KM, Chang HH, Muscatello DJ, Palekar R, Tempia S, *et al*. Estimates of global seasonal influenza-associated respiratory mortality: a modelling study. Lancet. 2018; 391: 1285–1300.

[4] Morens DM, Taubenberger JK, Fauci AS. Predominant role of bacterial pneumonia as a cause of death in pandemic influenza: implications for pandemic influenza preparedness. The Journal of Infectious Diseases. 2008; 198: 962–970.

[5] Ortiz JR, Neuzil KM, Rue TC, Zhou H, Shay DK, Cheng PY, *et al*. Population-based incidence estimates of influenza-associated respiratory failure hospitalizations, 2003 to 2009. American Journal of Respiratory and Critical Care Medicine. 2013; 188: 710–715.

[6] Short KR, Kroeze EJBV, Fouchier RAM, Kuiken T. Pathogenesis of influenza-induced acute respiratory distress syndrome. The Lancet. Infectious Diseases. 2014; 14: 57–69.

[7] Kuiken T, Taubenberger JK. Pathology of human influenza revisited. Vaccine. 2008; 26: D59–D66.

[8] Huertas A, Guignabert C, Barberà JA, Bärtsch P, Bhattacharya J, Bhattacharya S, *et al*. Pulmonary vascular endothelium: the orchestra conductor in respiratory diseases: Highlights from basic research to therapy. The European Respiratory Journal. 2018; 51: 1700745.

[9] Riscili BP, Anderson TB, Prescott HC, Exline MC, Sopirala MM, Phillips GS, *et al*. An assessment of H1N1 influenza-associated acute respiratory distress syndrome severity after adjustment for treatment characteristics. PLoS ONE. 2011; 6: e18166.

[10] Bautista E, Chotpitayasunondh T, Gao Z, Harper SA, Shaw M, Uyeki TM, *et al*. Clinical aspects of pandemic 2009 influenza A (H1N1) virus infection. The New England Journal of Medicine. 2010; 362: 1708–1719.

[11] Iwasaki A, Pillai PS. Innate immunity to influenza virus infection. Nature Reviews. Immunology. 2014; 14: 315–328.

[12] Herold S, Becker C, Ridge KM, Budinger GRS. Influenza virus-induced lung injury: pathogenesis and implications for treatment. The European Respiratory Journal. 2015; 45: 1463–1478.

[13] Taubenberger JK, Morens DM. The pathology of influenza virus infections. Annual Review of Pathology. 2008; 3: 499–522.

[14] Hedlund E, Deng Q. Single-cell RNA sequencing: Technical advancements and biological applications. Molecular Aspects of Medicine. 2018; 59: 36–46.

[15] Papalexi E, Satija R. Single-cell RNA sequencing to explore immune cell heterogeneity. Nature Reviews. Immunology. 2018; 18: 35–45.

[16] Steuerman Y, Cohen M, Peshes-Yaloz N, Valadarsky L, Cohn O, David E, *et al*. Dissection of Influenza Infection In Vivo by Single-Cell RNA Sequencing. Cell Systems. 2018; 6: 679–691.e4.

[17] Horns F, Dekker CL, Quake SR. Memory B Cell Activation, Broad Anti-influenza Antibodies, and Bystander Activation Revealed by Single-Cell Transcriptomics. Cell Reports. 2020; 30: 905–913.e6.

[18] Lee MN, Ye C, Villani AC, Raj T, Li W, Eisenhaure TM, *et al*. Common genetic variants modulate pathogen-sensing responses in human dendritic cells. Science. 2014; 343: 1246980.

[19] Quach H, Rotival M, Pothlichet J, Loh YHE, Dannemann M, Zidane N, *et al*. Genetic Adaptation and Neandertal Admixture Shaped the Immune System of Human Populations. Cell. 2016; 167: 643–656.e17.

[20] Jiang RD, Liu MQ, Chen Y, Shan C, Zhou YW, Shen XR, *et al*. Pathogenesis of SARS-CoV-2 in Transgenic Mice Expressing Human Angiotensin-Converting Enzyme 2. Cell. 2020; 182: 50–58.e8.

[21] Deng W, Bao L, Liu J, Xiao C, Liu J, Xue J, *et al*. Primary exposure to SARS-CoV-2 protects against reinfection in rhesus macaques. Science. 2020; 369: 818–823.

[22] Sano E, Suzuki T, Hashimoto R, Itoh Y, Sakamoto A, Sakai Y, *et al*. Cell response analysis in SARS-CoV-2 infected bronchial organoids. Communications Biology. 2022; 5: 516.

[23] Han Y, Yang L, Lacko LA, Chen S. Human organoid models to study SARS-CoV-2 infection. Nature Methods. 2022; 19: 418–428.

[24] Masopust D, Sivula CP, Jameson SC. Of Mice, Dirty Mice, and Men: Using Mice To Understand Human Immunology. Journal of Immunology. 2017; 199: 383–388.

[25] de Souza N. Model organisms: Mouse models challenged. Nature Methods. 2013; 10: 288.

[26] Perlman RL. Mouse models of human disease: An evolutionary perspective. Evolution, Medicine, and Public Health. 2016; 2016: 170–176.

[27] Mestas J, Hughes CCW. Of mice and not men: differences between mouse and human immunology. Journal of Immunology. 2004; 172: 2731–2738.

[28] Clevers H. Modeling Development and Disease with Organoids. Cell. 2016; 165: 1586–1597.

[29] Jalili-Firoozinezhad S, Miranda CC, Cabral JMS. Modeling the Human Body on Microfluidic Chips. Trends in Biotechnology. 2021; 39: 838–852.

[30] Bhatia SN, Ingber DE. Microfluidic organs-on-chips. Nature Biotechnology. 2014; 32: 760–772.

[31] Huh DD. A human breathing lung-on-a-chip. Annals of the American Thoracic Society. 2015; 12: S42–S44.

[32] Stucki AO, Stucki JD, Hall SRR, Felder M, Mermoud Y, Schmid RA, *et al*. A lung-on-a-chip array with an integrated bio-inspired respiration mechanism. Lab on a Chip. 2015; 15: 1302–1310.

[33] Gkatzis K, Taghizadeh S, Huh D, Stainier DYR, Bellusci S. Use of three-dimensional organoids and lung-on-a-chip methods to study lung development, regeneration and disease. The European Respiratory Journal. 2018; 52: 1800876.

[34] van Meer BJ, de Vries H, Firth KSA, van Weerd J, Tertoolen LGJ, Karperien HBJ, *et al*. Small molecule absorption by PDMS in the context of drug response bioassays. Biochemical and Biophysical Research Communications. 2017; 482: 323–328.

[35] Ashammakhi N, Nasiri R, Barros NRD, Tebon P, Thakor J, Goudie M, *et al*. Gut-on-a-chip: Current progress and future opportunities. Biomaterials. 2020; 255: 120196.

[36] Brandes S, Dietrich S, Hünniger K, Kurzai O, Figge MT. Migration and interaction tracking for quantitative analysis of phagocyte-pathogen confrontation assays. Medical Image Analysis. 2017; 36: 172–183.

[37] Brandes S, Mokhtari Z, Essig F, Hünniger K, Kurzai O, Figge MT. Automated segmentation and tracking of non-rigid objects in time-lapse microscopy videos of polymorphonuclear neutrophils. Medical Image Analysis. 2015; 20: 34–51.

[38] Huh D, Matthews BD, Mammoto A, Montoya-Zavala M, Hsin HY, Ingber DE. Reconstituting organ-level lung functions on a chip. Science. 2010; 328: 1662–1668.

[39] Vunjak-Novakovic G, Ronaldson-Bouchard K, Radisic M. Organs-on-a-chip models for biological research. Cell. 2021; 184: 4597–4611.

[40] Zhang M, Wang P, Luo R, Wang Y, Li Z, Guo Y, *et al*. Biomimetic Human Disease Model of SARS-CoV-2-Induced Lung Injury and Immune Responses on Organ Chip System. Advanced Science. 2020; 8: 2002928.

[41] Benam KH, Villenave R, Lucchesi C, Varone A, Hubeau C, Lee HH, *et al*. Small airway-on-a-chip enables analysis of human lung inflammation and drug responses in vitro. Nature Methods. 2016; 13: 151–157.

[42] Huh D, Leslie DC, Matthews BD, Fraser JP, Jurek S, Hamilton GA, *et al*. A human disease model of drug toxicity-induced pulmonary edema in a lung-on-a-chip microdevice. Science Translational Medicine. 2012; 4: 159ra147.

[43] Hubatsch I, Ragnarsson EGE, Artursson P. Determination of drug permeability and prediction of drug absorption in Caco-2 monolayers. Nature Protocols. 2007; 2: 2111–2119.

[44] Vento-Tormo R, Efremova M, Botting RA, Turco MY, Vento-Tormo M, Meyer KB, *et al*. Single-cell reconstruction of the early maternal-fetal interface in humans. Nature. 2018; 563: 347–353.

[45] Wang J, Edeen K, Manzer R, Chang Y, Wang S, Chen X, *et al*. Differentiated human alveolar epithelial cells and reversibility of their phenotype in vitro. American Journal of Respiratory Cell and Molecular Biology. 2007; 36: 661–668.

[46] Herzog EL, Brody AR, Colby TV, Mason R, Williams MC. Knowns and unknowns of the alveolus. Proceedings of the American Thoracic Society. 2008; 5: 778–782.

[47] Hutchinson EC. Influenza Virus. Trends in Microbiology. 2018; 26: 809–810.

[48] Neuzil KM, Victor JC. Annual studies of influenza vaccine effectiveness: evaluating performance, informing policy, and generating new questions. Clinical Infectious Diseases. 2014; 58: 328–329.

[49] Smith CA, Tyrell DJ, Kulkarni UA, Wood S, Leng L, Zemans RL, *et al*. Macrophage migration inhibitory factor enhances influenza-associated mortality in mice. JCI Insight. 2019; 4: e128034.

[50] Goraya MU, Wang S, Munir M, Chen JL. Induction of innate immunity and its perturbation by influenza viruses. Protein & Cell. 2015; 6: 712–721.

[51] Chow EJ, Doyle JD, Uyeki TM. Influenza virus-related critical illness: prevention, diagnosis, treatment. Critical Care. 2019; 23: 214.

[52] Moesta AK, Parham P. Diverse functionality among human NK cell receptors for the C1 epitope of HLA-C: KIR2DS2, KIR2DL2, and KIR2DL3. Frontiers in Immunology. 2012; 3: 336.

[53] Shannon LA, McBurney TM, Wells MA, Roth ME, Calloway PA, Bill CA, *et al*. CCR7/CCL19 controls expression of EDG-1 in T cells. The Journal of Biological Chemistry. 2012; 287: 11656–11664.